Introducing Passive Nuclear Safety in Water-Cooled Reactors: Numerical Simulation and Validation of Natural Convection Heat Transfer and Transport in Packed Beds of Heated Microspheres

Olugbenga O. Noah[1], Johan F. Slabber[2], Josua P. Meyer[3]

Department of Mechanical and Aeronautical Engineering, University of Pretoria,
Private Bag X20, Hatfield, Pretoria 0028, South Africa

[1]Corresponding author. e-mail: Noah.Olugbenga@tuks.co.za
[2]Corresponding author. e-mail: johan.slabber@up.ac.za
[3]Corresponding author. e-mail: josua.meyer@up.ac.za

Abstract

The development of an accident tolerant nuclear fuel for water-cooled reactors would redefined the status of these reactors from traditional active safety to passive safety systems. As a possible solution toward enhancing the safety of light-water reactors (LWRs), loose-coated particles of enriched uranium dioxide (UO_2) fuel with the ability to retain gaseous and metallic fission products in the case of a loss of cooling event can be introduced inside Silicon-Carbide cladding tubes of the fuel assembly (see Figs. 1(a) and 1(b)). These coated particles are treated as a bed from where heat is transferred to the cladding tube and the helium gas movement is due to natural convection. A slender geometrical model with tube-to-particle diameter ratio N = 2.503 and porosity $\varepsilon = 0.546$ mimicking the proposed nuclear fuel in the cladding was numerically simulated. This study is to investigate the heat transfer characteristics and flow distribution under buoyancy driven force expected in the cladding tube of the proposed nuclear fuel using a commercial code. Random packing of the particles is achieved by discrete element method (DEM) simulation with the aid of STARCCM+. The temperature contour and velocity vector plots obtained can be said to be good illustration of anticipated heat transfer and transport phenomenon to occur in the proposed fuel design. Simulated results for particle-to-fluid heat transfer coefficient, Nusselt number, and Rayleigh number which are of prime importance when analyzing natural convection heat transfer performance in fixed bed reactors were validated. Results from this work show close agreement with results obtained in established numerical and experimental works.

Keywords: light water reactor, active and passive safety, numerical simulation, natural convection heat transfer, nuclear fuel

1 Introduction

A number of innovative reactor systems are being developed currently around the globe. Amongst these systems is the high temperature reactor (HTR) utilizing pebble shaped fuel elements and helium as the working gas [1]. The heat transfer in particle-to-fluid packed bed systems is important in high temperature nuclear reactors utilizing the pebble fuel concept. Hence extensive knowledge and thorough understanding of the heat transfer in porous media is essential for successful design of such systems and also in modified water cooled reactors applying the HTR fuel concept such as the one being proposed in this study. Because of the importance of particle-to-fluid heat transfer characteristics in high temperature reactors, a considerable effort has been made to evaluate these parameters [2]. Experimental determination of heat transfer characteristics for a wide variety of systems have been made using various experimental techniques, under either steady-state or unsteady-state conditions. Some theoretical studies carried out were used to explain experimental results and correlations that were established [3].

The ability of coated particles of enriched uranium dioxide fuel to withstand high temperature and contain radioactive fission products in the case of a loss of cooling event is a vital passive safety measure over traditional nuclear fuel [4]. In an attempt to enhance the safety of light water reactors, a new nuclear fuel design for light water reactors is being proposed; the fuel in the form of loose coated particles in a Helium environment is introduced inside the cladding tubes. In the process of developing this concept, this study tends to investigate particle-to-fluid heat transfer characteristics and flow distribution under natural convective conditions that is anticipated in slender beds of randomly packed heated spheres (coated fuel particles) through the use of computational fluid dynamics (CFD) simulations.

In recent years, the use of numerical simulation through CFD is growing and this offers the opportunity to predict the heat transfer and fluid flow phenomena in packed beds. This thereby provides important gain of time, limit the number of experiments, and accessing information at a large scale which may not be measurable with experimental methods. It is also possible to take into account real physical properties such as high temperature and pressure conditions [5]. The main limitation of heat transfer models in packed beds is the poor knowledge about flow patterns within them, the use of modeling and simulation tools have made it

possible to define not only spatial distribution of involved species, but also temperature and velocity profiles within the bed. Although confronted in the past with microprocessor speed, memory size and computational time, consistent gains over the years in these deterrent areas has made highly accurate and computationally expensive computer codes more practical in simulating system behavior in modern nuclear reactors.

The use of CFD to predict heat or mass transfer coefficients has been applied in a lot of different packed bed configurations but most are faced with problems ranging from porosity [6], contact points and accurate meshing of models [7]. In most past studies considered, problem arises as a result of improper meshing of contact points between particles when finite volume methods are used to simulate the flow between particles. This necessitated contracting the particle diameter to permit CFD calculations but the contraction of spheres increases the porosity of the bed which affects the pressure drop in the medium. This is detrimental to the quality of the results obtained from such a model. Pressure drop, particle-to-fluid heat and mass transfer in low channel to particle diameter ratio was studied [8,9] to show that commercial CFD codes can be used to adequately predict particle-to-fluid heat transfer of a single free sphere. A simple model consisting of three spheres in a tube was later developed to investigate the wall heat transfer coefficients [10]. Logtemberg and Dixon [11] extended this model to eight spheres, divided into two layers of four spheres without solid–solid contact points. However, Ref. [12] incorporated contact points between the solids in a ten-sphere model, which used spherical dead volumes around the contact points. This model showed flow and heat transfer behavior that could not be described by the conventional fixed bed model. Simulations have been presented also for model geometry of 44 solid spheres in a tube with tube-to-particle diameter ratio equal to 2 [13]. Conclusion from these and other researches indicate that applying gaps or overlaps methods at contact points of wall-to-particle and particle-to-particle would change the bed porosity and give erroneous results while bridges or capes methods would make little deviations in the porosity and give reasonable results, such as in the prediction of drag coefficient and pressure drops. A new and more realistic method is introduced and applied in this work.

In this study, a geometrical model of the bed containing 171 uniformly sized particles randomly packed in an enclosed slender cylindrical tube is modeled and analyzed at a particle maximum surface temperature of 700 K. The model mimicking the proposed nuclear fuel in the cladding is numerically simulated to investigate the heat transfer characteristics and flow distribution under the natural convective conditions anticipated in beds of randomly packed spheres (coated fuel particles) using a commercial code. Random packing of the particles was achieved by discrete element method (DEM) simulation with the aid of STARCCM+ while particle-to-particle and particle-to-wall contacts was achieved through the combined use of the commercial code and a SOLIDWORKSCAD package. Methodologies adopted and models described in this paper are original concept established by authors of this paper in the course of this research.

2 Proposed Fuel and Basic Considerations

2.1 Proposed Accident Tolerant Nuclear Fuel.

Accidents resulting in the release of radioactive fission products are principally driven by the degradation of the barrier due to excessive temperature. The concept of the new design proposed in this study (see Fig. 1(c)) is to redesign the present nuclear fuel (see Fig. 1(d)) into a form of loose coated particles in a helium atmosphere inside the cladding tube of the fuel elements (see Fig. 1(b)). In the proposal, coated particles of enriched uranium dioxide (UO_2) fuel (kernel), 0.5 mm in diameter, are coated with two-layers; pyrolytic carbon (PyC) layer which serves as buffer coating to absorb the fission gases, silicon carbide (SiC) layer is to retain the fission gas pressure and form together a barrier against all fission products. The two-layers are to provide the primary barrier to fission product release. Coated particles are loaded in the cladding tube and filled to the brim leaving no provision for plenum at the top.

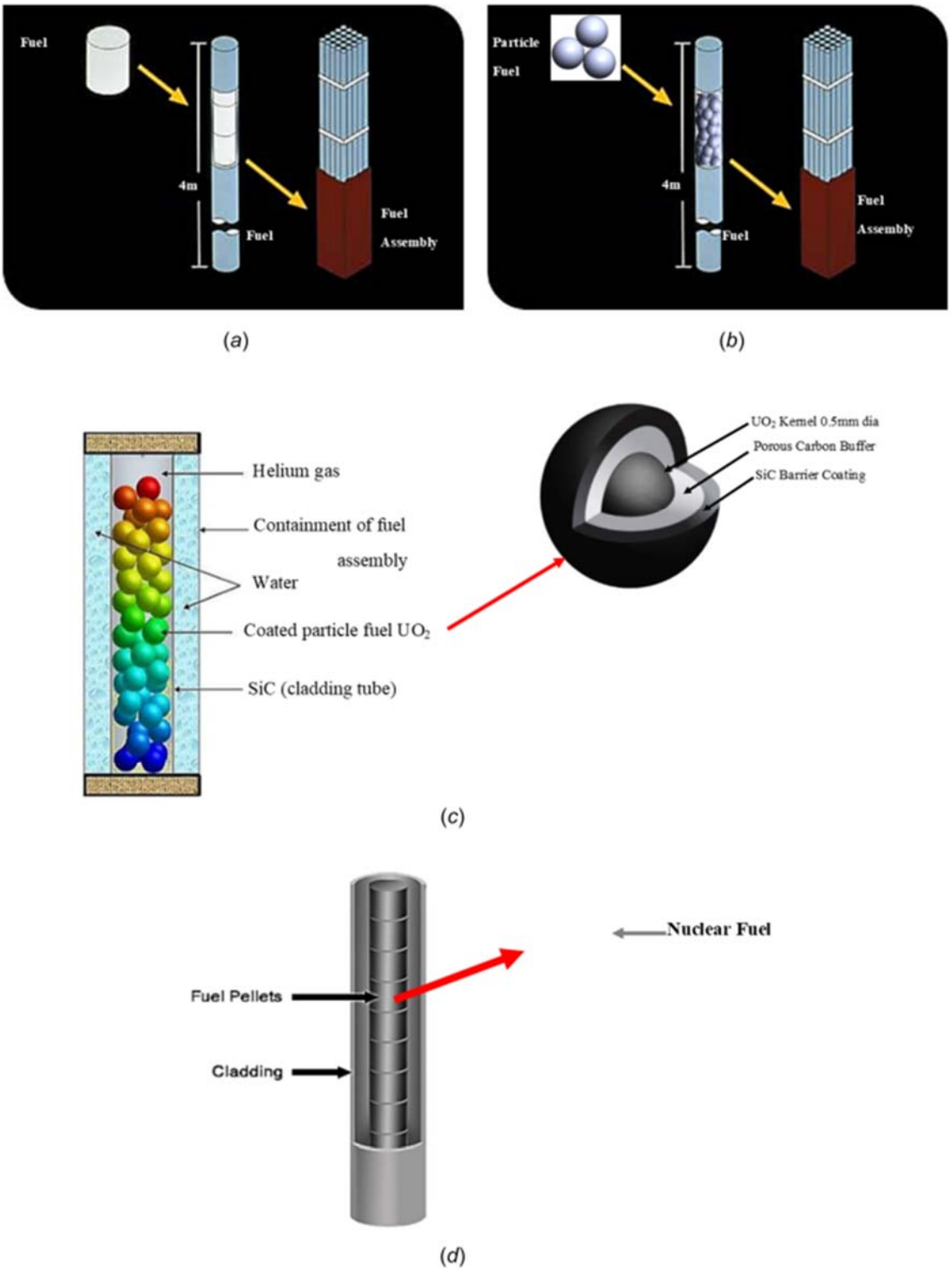

Fig. 1. (*a*) Traditional nuclear fuel assembly, (*b*) proposed new nuclear fuel design, (*c*) schematics of proposed coated particle fuel design in a SiC cladding tube, and (*d*) schematics of traditional fuel in cladding tube

In practical operation, filling the cladding tube with coated particles is expected to be quicker and easier than filling the traditional nuclear fuel considering the filling technique intended to be used. Although the traditional nuclear fuel is expected to have higher packing density in the tube than the proposed fuel design, a make-up in short-fall of fuel content is achieved by merely increasing the enrichment proportionally but not beyond 15%. On the other hand, higher fuel enrichment in the proposed nuclear fuel will provide higher burn-up, which is another advantage of the proposed design over the traditional nuclear fuel. Production cost of the proposed coated particles is expected to be cheaper compared to the traditional nuclear fuel (fuel pellet). Apart from the passive safety system advantage the proposal has over the traditional nuclear fuel, the risk of rod breakage in case of some accident is expected to be lower. The maximum fuel temperatures during normal operation are usually around $700 - 800\ ^{o}\mathrm{C}$ but under accident conditions, the proposed coated particles fuel is expected to remain leak-tight (sealed) till much higher temperatures of around 1600 °C.

2.2 Particle-to-Fluid Heat Transfer.

The first step in the solution of fixed bed flow and heat transfer problems in complex geometry is to solve the problem of one sphere suspended in an infinite domain of fluid. Basic simulation knowledge of particle-to-fluid heat transfer for a single free sphere in an "infinite" fluid domain is considered necessary for better understanding of simulating packed particles in a tube. Considering a single free sphere in a medium simulated using CFD for particle-to-fluid heat transfer rate, *Q*. The temperature of the surface of the particle is set to a surface temperature T_p while the fluid at the boundary of the domain is set to a lower bulk temperature, T_∞. As a result of the temperature difference between the particle surface and the fluid, heat is transferred from the particle to the fluid. For each simulation, temperature contour plots were analyzed, and heat flux through the particle surface was recorded. With this data the particle-to-fluid average heat transfer coefficient $\overline{h}$ could be determined as expressed by the following equation:

$$\overline{h} = \frac{\bar{q}''}{T_p - T_\infty} = \frac{\overline{Q}}{\pi d_p^2 (T_p - T_\infty)} \quad (1)$$

The average Nusselt number of the single particle is expressed by the following equation:

$$\overline{\mathrm{Nu}} = \frac{\bar{h} d_p}{k_f} = \frac{\bar{Q}}{\pi d_p k_f (T_p - T_\infty)} \tag{2}$$

This model works well for simple cases, like a single free sphere, where the temperature difference between the surface and the bulk temperature is well defined. However, it is less applicable to packed beds because the bulk temperature is not easily defined [9]. In packed beds with a constant particle surface temperature, the resistance to heat transfer resides only on the fluid side. Theoretical analysis shows that if axial fluid thermal dispersion is taken into consideration, then, a conservative heat energy balance equation can be established [4] and the heat transfer coefficient deduced. For packed beds contained in an enclosed tube with a given particle surface temperature T_P like the case under investigation, Q_{nu} is considered as the heat generated by nuclear fission in the coated particle fuel, $\overline{N}_c$ is the frequency distribution of the number of contact points which in most cases is referred to as the average coordination number or *average kissing number* [14] which is a function of bulk porosity, R_G is the thermal resistance of the interstitial gas in the macrogap. Considering a basic unit cell in the medium of the proposed new fuel design, the convectional engineering expression developed in the course of this research for the particle-to-fluid heat transfer coefficient h_{pf} [4] is given in Eq. (3). For each simulation, temperature, thermal conductivities and density profiles along the bed were recorded and analyzed. With the collected data, h_{pf} was obtained from the following equation:

$$h_{\mathrm{pf}} = \frac{Q_{\mathrm{nu}} - \left(1-\varepsilon\right)\frac{(\rho c_{\mathrm{p}} V_T)\Delta T}{\Delta t} - \left\{N_c\left[k_{\mathrm{eff}}^c \frac{dT}{dz} A_c + \frac{\Delta T}{R_G}\right] - A_{\mathrm{p}} q_R''\right\}}{\left(A_p - \overline{N}_c A_c\right)\left(T_p - T_f\right)} \tag{3}$$

where ε

where ε, k_{eff}^c, q_R'', A_{p}, A_c represent the bed porosity, the effective thermal conductivity at the contact interface between particles, the radiative heat flux, the spherical particle total surface area, and the area of contact spot, respectively.

2.3 Transport Phenomenon.

Computation of flow is achieved by mathematical models based upon conservation principles, namely, the conservation of mass, momentum and energy governed by the 3D Navier–Stokes equations representing the fluid as a continuum for an arbitrary control volume. Natural convection is generated by the density differences induced by the temperature differences within a fluid system. Using the physical (interstitial) formulation and assuming a general scalar Ø, the governing equation in an isotropic porous region expressed in differential form is shown in Eq. (4). Discrete versions of the integral form of the continuum transport equations were applied to each control volume. The objective was to obtain a set of linear algebraic equations, with the total number of unknowns in each equation system corresponding to the number of cells in the grid. With nonlinear equation, iterative techniques that rely on suitable linearization strategies must be employed. The resulting linear equations are then solved with an algebraic multigrid solver. Considering the general governing equation given in Eq. (4) which consists of the transient term, convective term, diffusion term and the source term, respectively, the Discretization approach for individual term differs. The transient term is only included in transient calculations, it is not generally used as a device to obtain a steady-state solution

$$\frac{\partial(\varepsilon\rho\emptyset)}{\partial t} + \nabla\cdot\left(\varepsilon\rho\mathbf{v}\emptyset\right) = \nabla\cdot\left(\varepsilon\Gamma\nabla\emptyset\right) + \varepsilon S_{\emptyset} \tag{4}$$

For isotropic porosity and single phase flow, the volume-averaged mass and momentum conservation equations are expressed by the following equations:

$$\frac{\partial(\varepsilon\rho)}{\partial t} + \nabla\cdot\left(\varepsilon\rho\mathbf{v}\right) = 0 \tag{5}$$

$$\frac{\partial(\varepsilon\rho\mathbf{v})}{\partial t} + \nabla\cdot\left(\varepsilon\rho\mathbf{v}\mathbf{v}\right) = -\varepsilon\nabla p + \nabla\cdot\left(\varepsilon\boldsymbol{\tau}\right) + \varepsilon\mathbf{B}_f - \left(\frac{\varepsilon^2\mu}{K}\mathbf{v} + \frac{\varepsilon^3 C_2}{2}\rho|\mathbf{v}|\mathbf{v}\right) \tag{6}$$

The CFD code solves the full set of discretized Navier–Stokes equation using a finite volume approach. The last term in Eq. (6) is the porous source term in the momentum equation; it is made up of the viscous and inertial drag forces imposed by the pore walls on the fluid. The commercial code uses an iterative procedure to reach the solution to the transport equations that satisfies the boundary conditions for the study. The mechanics of continua (both solid and fluid) are described by transport equations derived from the assumption that mass, momentum and energy

are conserved in the continuum.

3 Geometrical Models

3.1 Packing of Spherical Particles in the Tube.

Random particle packings can be built by means of different methods. These methods are essentially of two types: deposition algorithms and dynamic simulation method known as DEM. Deposition algorithms are generally very quick but provide samples that are mechanically unstable. Furthermore, these algorithms are not suitable for the construction of very dense packings such as a granular bed obtained by deposition under gravity. In this work, a discrete element method simulation was used to construct a densely packed cylindrical sample composed of spherical particles. Geometrical model of the proposed new fuel design is developed with the aid of a commercial CFD code for the DEM simulation (see Fig. 2) and a computer aided design (CAD) package for creating contact points between adjacent packed particles by expansion of packed bed particles diameter. DEM is an engineering numerical method used to simulate motion of a large number of interacting discrete objects which are typically solid particles. DEM model established by Ref. [15] is an extension of Lagrangian modeling methodology to include dense particle flows; STARCCM+ uses a classical mechanics method to model DEM and is based on soft-particle formulation where particles are allowed to develop an overlap [16]. The numerical sample is very similar to the experimental close-packed materials and its solid fraction can be adjusted by the tuning friction or cohesion between particles [17,18]. Before generating and packing particles, a particle diameter needs to be chosen, this diameters can be exactly the same as in the experiments practice. Uniform Particles of 15.9 mm diameter and a cylinder of 40 mm diameter are used in this study for the DEM simulation.

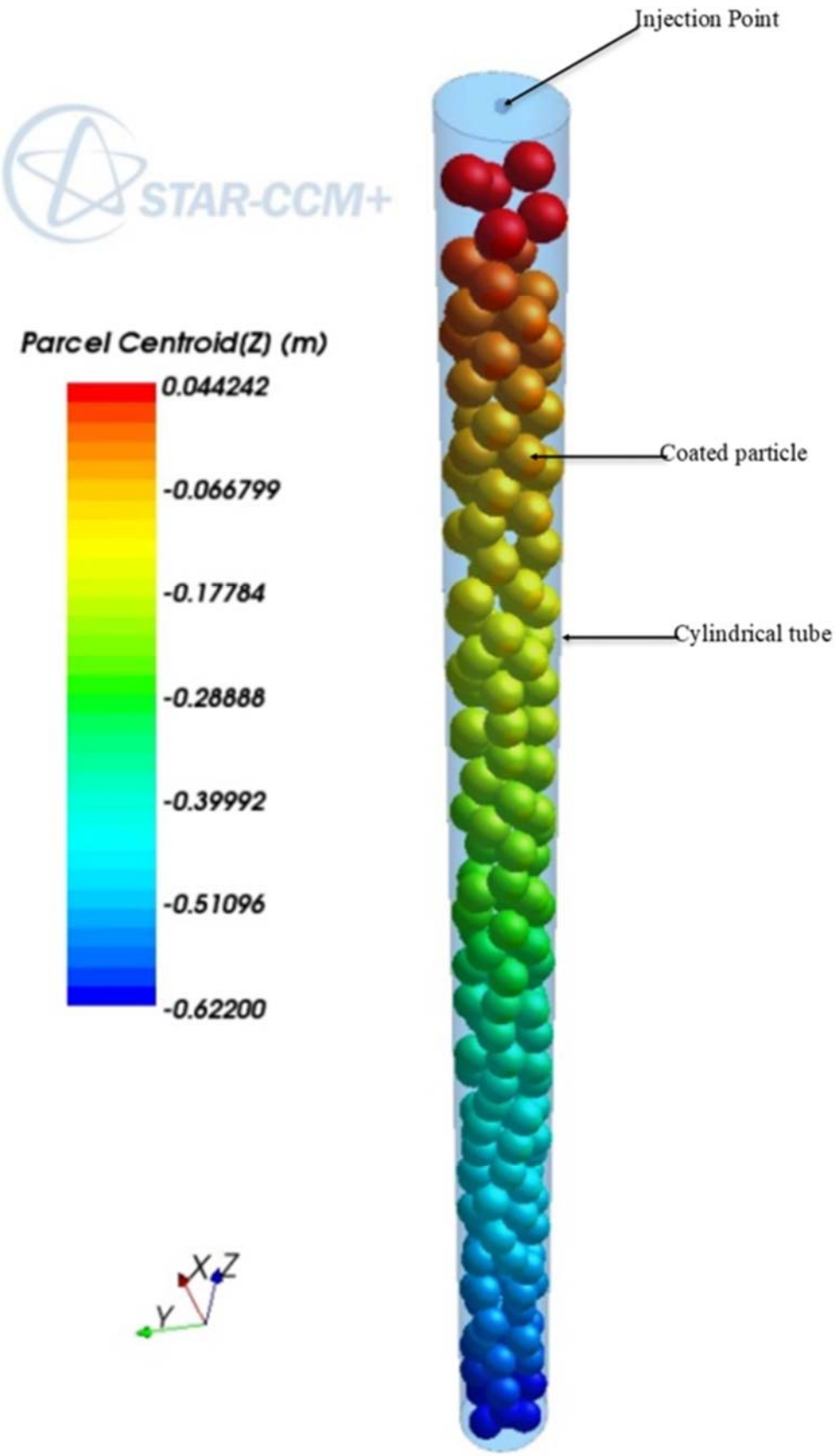

Fig. 2. DEM simulated randomly packed particles

A single injector with random point distribution was used to inject particles (raining of particles) into an enclosed tube (see Fig. 2). The amount of injected particles is controlled by the porosity limit property. During the raining process, a loose (and nonphysical) packing is generated. The forces at the point of contact are modeled as a pair of spring-dashpot oscillators; one representing the normal direction and the other the tangential direction of force with respect to the contact plane normal vector. The force $\mathbf{F}_c$ between two spheres described by Eq. (7) has a normal part $\mathbf{F}_n$ due to the presence of contacts between particles and a tangential part $\mathbf{F}_t$ due to friction (see Fig. 3(a)). The two parts are expressed by Eqs. (8) and (9)

$$\mathbf{F}_c = \mathbf{F}_n + \mathbf{F}_t \tag{7}$$

For the force law between a pair of contacting particles, we use a linear-elastic approximation [7]

$$\mathbf{F}_n = \left(-k_n\delta + 2\alpha\sqrt{m\mathrm{k}_n}\,\dot{\delta}\right)\frac{C_i\vec{C}_j}{\|\mathbf{C_iC_j}\|} \quad \text{for} \quad \delta < 0 \tag{8}$$

and $\mathbf{F}_n = 0$ otherwise. $\delta = \left\|\mathbf{C_iC_j}\right\| - \frac{1}{2}\left(d_i + d_j\right)$ is the gap (see Fig. 3(b)) or the overlap between the two contacting particles *i* and *j* (Fig. 3(a)), $\mathbf{k}_n$ is the normal stiffness, $m = m_i m_j / m_i + m_j$ is the reduced mass and $\alpha\epsilon[0, 1]$ is a damping parameter which controls energy dissipation due to inelastic collision [7]. Since there is an interest in the equilibrium state, the parameter α has a very weak influence on the final results, but high values of α reduces the simulation time. For the friction, the classical Coulomb law was used and expressed as a nonlinear relation between the friction force $\mathbf{F}_t$ and the sliding velocity $\boldsymbol{\delta}_t$ with a viscous regularization around the zero velocity

$$\mathbf{F}_t = -\min\left\{\beta_t\left\|\dot{\boldsymbol{\delta}}_t\right\|, \mu_c\|\mathbf{N}\|\right\}\frac{\dot{\delta}_t}{\|\dot{\delta}_t\|} \tag{9}$$

where β_t is the tangential viscosity parameter and μ_c is the coefficient of friction [7], values of some of these parameters are displayed in Table 1 Similar force laws are used to compute the interactions of the grains with the top and upper plates and with the inner wall of the cylindrical column [19].

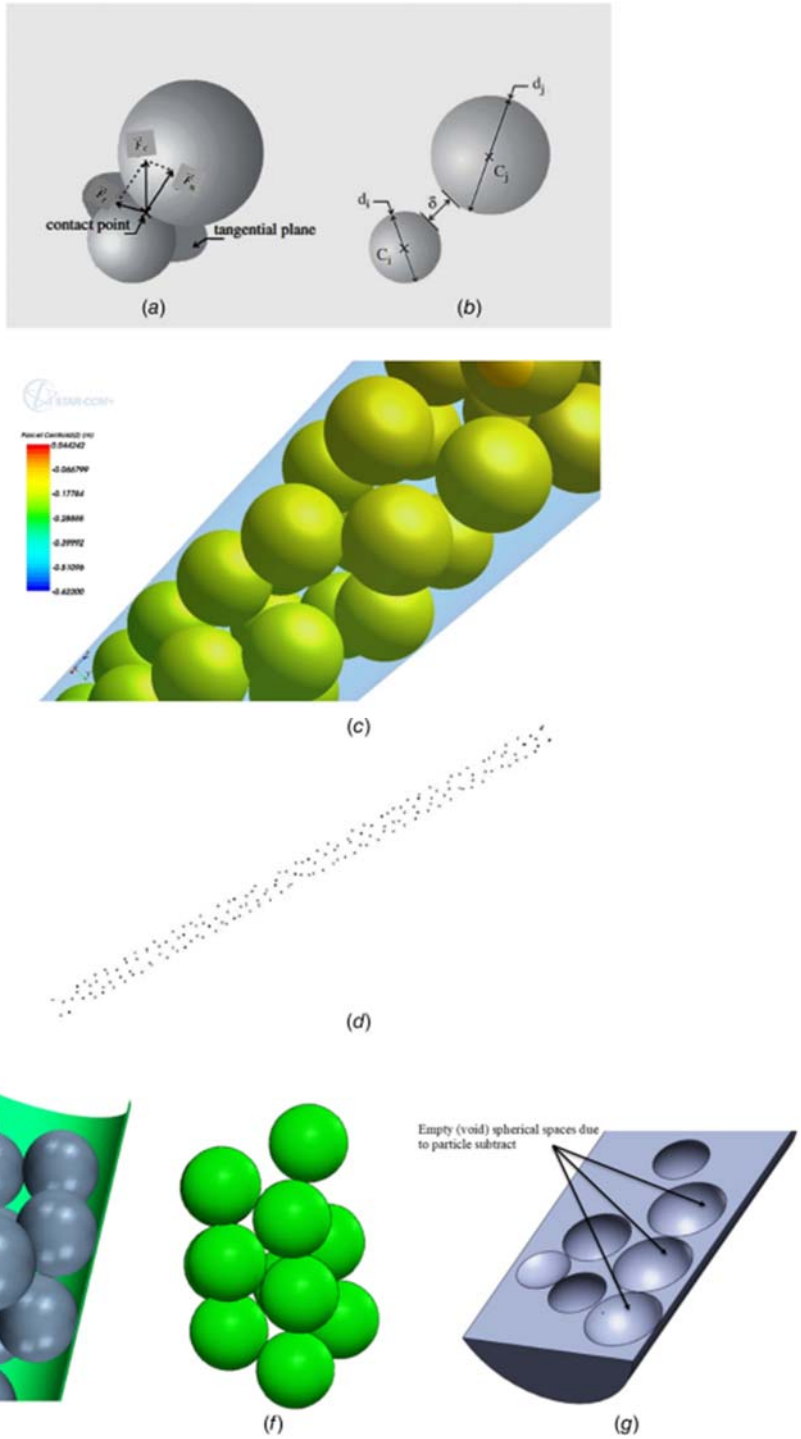

Fig. 3. (*a*) Contact force components between particles, (*b*) Geometrical parameters and gap between two particles, (*c*) DEM simulation model with gap between two particles and gaps between wall and particles, (*d*) DEM simulation centroid coordinate points (*x, y, z*) in CAD environment, (*e*) packed particles diameter expansion for creation of contacts; between adjacent particles, and between walls and particles using CAD, (*f*) packed particles subtract (solid region), and (*g*) sectional plane of fluid domain after Boolean subtract operation (fluid region)

Table 1

Parameters for DEM packing

Parameter	Value
Normal stiffness, k_n (N/m)	1×10^6
Interparticle friction coefficient, μ_c	μ_c 0.3
Density of particles, ρ_p ($\mathbf{kg/m^3}$)	$\mathbf{2250}$
Damping coefficient, α	0.7
Tangential viscosity, β (Ns/m)	1
Time step ($\mathbf{sec}$)	5×10^{-5}

Given the local interaction laws, the algorithm for the simulation of a collection of particles follows the following general scheme: (1) at each time-step, the displacements of the particles are used to compute the forces between grains and with boundary walls, (2) the accelerations are determined by means of the equations of motion from forces acting on the particles, (3) the "velocity verlet" scheme [20] is used for the integration of the equations of motion over a time-step in order to calculate the particle displacements, and (4) the grain positions are updated according to the calculated displacements. The friction between particles and the inner wall of the cylindrical mold is neglected. The simulation was stopped when a dense packing is formed and the particles fit to the cylindrical geometry (Fig. 2). For this study, 171 densely packed uniformly sized particles with packing ratio of 0.58 were generated by the DEM simulation.

The construction of wall-to-particle and particle-to-particle contact points is also an important subject in the process of developing a geometrical model. Previous work in literature reports the emulation of contact points (leaving small gaps between surfaces and assuming zero velocity in the gap) to avoid convergence problems [13]. In this study, to establish real particle-to-particle and particle-to-wall contact points, a 0.5% particle diameter expansion is carried out on each bed particle to create an existence of a small overlapping between particles. Convergence problems were not detected during simulation runs.

3.2 Computer Aided Design operation and Contacts Creation.

For appropriate volume mesh generation to be carried out on the geometry, some work needed to be done on the DEM simulated randomly packed particles to close-up the existing gap between adjacent particles and also between the walls and particles (see Fig. 3(c)). The *x*-, *y*-, and *z*-centroid coordinate points of all the packed particles obtained through the *XY* plot are extracted from the STARCCM+ environment to an excel spread sheet. The centroid points of all the 171 particles are then imported from the excel spread sheet through the use of a macrovisual basic program into a SOLIDWORKS (CAD) environment (see Fig. 3(d)). Particles with 0.5% diameter increment (expansion to create small overlapping between particles) are drawn on each centroid to generate particle-to-particle and particle-to-wall contacts (see Fig. 3(e)). A Boolean subtract operation is carried out to cut out the packed particles (solid spheres) in the cylinder fluid region. Boolean operation is done to subtract the spheres (see Fig. 3(f)) from the cylinder leaving empty spherical spaces (void) in the cylinder (see Fig. 3(g)). The cylinder fluid region and the packed particles (subtract) which is herewith referred to as the solid region are simultaneously exported back to STARCCM+ for surface and volume mesh generation. Heat transfer performance calculations are carried out using the modified particles size.

4 Mesh Design, Simulation, and Model Analysis

4.1 Mesh Design.

The mesh establishes the accuracy of the simulation which has to be chosen with enough detail to describe the simulation processes accurately. The cylinder fluid region and the packed spheres solid region (subtracts) are simultaneously exported back to the commercial code software from the CAD package for volume mesh generation. A polyhedral mesh in conjunction with a prism layer mesh model was used to generate orthogonal prismatic cells next to wall boundaries (see Fig. 4). These layers of cells are necessary to allow the solver to resolve near wall flow accurately. This is critical in determining not only the forces and heat transfer on walls, but also flow features such as separation. On a mesh of given quality and sufficient fineness, higher-order schemes are applied for momentum and energy equations because it yields more accurate results than lower-order schemes. Grid skewing is an important contributing factor (much more than grid stretching) to the

loss in nominal accuracy of the solution. Skewed meshes found around the contact points though do not actually create serious problem for laminar solutions but it makes convergence in some specific cases unachievable when simulating turbulent flow. It turned out that the flow velocities, especially in the fluid elements around the contact points, are increasing dramatically, a very typical result for cells that are too skewed. Concerning the mesh sensitivity analysis, the test performed consisted in increasing the mesh density at the particle surface in order to properly capture the boundary layer associated problem. Four grid refinement levels are carried out in this study, from coarse to finer mesh. This is done by varying the mesh density to ensure that the CFD solution does not change with further mesh refinement as the aim of grid refinement is basically for numerical accuracy that leads to a solution closer to the exact solution of a system of equations that implies considerable physical approximations [21,22]. For a 1.0 mm base size used in this study, four sets of simulations were carried out within specified temperature range using varying mesh density and temperature profile results plotted. The results obtained for the last two finer meshes are almost identical (see Fig. 7), hence it can be established that simulations have reached an asymptotic solution and the geometry with the last grid refinement level of finer mesh density 2.0 is used to build the fixed bed model. The chosen geometry has 7,660,356 grid cells, 50,768,855 faces and 44,096,934 vertices; from experience, this should be adequate to capture heat transfer phenomena over the particle surfaces. An in-place interface is placed in-between the fluid and the solid region, this is to allow for appropriate transfer of quantities of mass and energy calculated during the simulation.

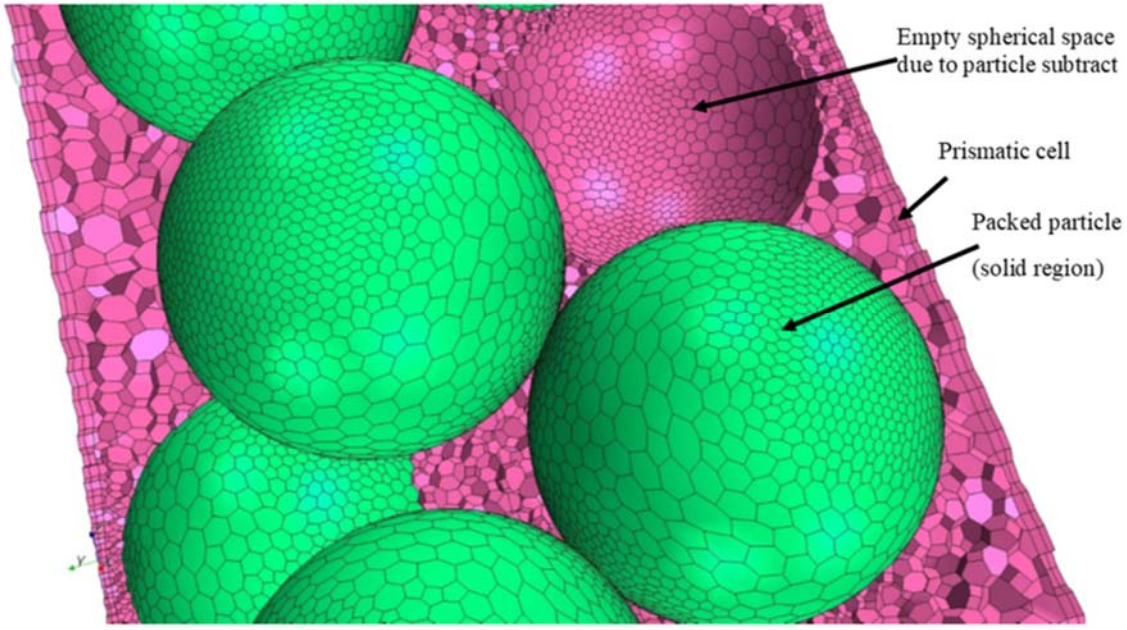

Fig. 4. Threshold of a generated quality mesh depicting particle-to-particle contacts in the fixed bed geometrical mode

4.2 Initial State and Boundary Conditions.

For a problem to be well posed, boundary conditions must be specified on all solution domain boundaries. Boundary conditions in this study are set the same as the boundary conditions anticipated in the proposed design. The working fluid in the model is specified as helium gas at initial static temperature 293.1 K, static gage pressure 0.0 Pa and reference pressure 101.325 kPa. The boundary conditions determine the flow and thermal variables on the boundaries of the physical model. The cylinder curved, top and bottom sides are set as walls, and temperature 300 K, cylinder wall thermal boundary condition is specified as environment due to expected heat transfer across the cladding tube wall and at no-slip wall conditions. The particles which form the solid region have their surfaces set as wall boundary at 700 K and thermal boundary condition specified as convection.

4.3 Simulation Run.

Used for this simulation, are 171 uniformly sized solid particles of 15.98 mm diameter each, and 2.503 tube-to-particle diameter ratio geometrical model. The particles are randomly packed in a helium gas environment contained in a slender cylindrical tube enclosed at both ends. The space model selected is 3D because; the mesh is

generated in three-dimensions, it described the physical model accurately and is able to handle the flow specifics of the packed bed geometry. For high pressure simulation, the gas was taken to be Newtonian, in the laminar flow regime and with variable density. Helium gas is chosen as the simulation fluid while coated particles surfaces is identified as graphite carbon and a thermal specification of 7500 W heat source is applied, the two porous materials have their thermal and material properties value available in the STARCCM+ database. The ideal gas law is used for the density temperature dependency and Sutherland's law [19] is used for the thermal conductivity and viscosity temperature dependencies. Gravitational acceleration is added to the operating conditions of the model. An implicit solver is applied in this implicit unsteady flow simulation. Its function is to control the update at each physical time for the calculation (solution of continuity, momentum and energy equations) and as well to control the time-step size. Segregated fluid energy and segregated models are applied for implicit unsteady flow. Appropriate numerical parameters (convergence limit, under relaxation factor, number of iterations/time-steps) are specified to control the calculation. A maximum step criteria of 100,000 was set as convergence limit, under-relaxation factor of 0.45 and time-step size of 0.00008 s were used in this study while simulation is runned at 20 iterations per time-step. Gray thermal Radiation model is specified for the surface-surface radiation expected at elevated temperatures. Simulation is run in a high end computer system (see Fig. 5) for close to 72 h. Numerical convergence of the model was checked based on a suitable diminution of the normalized numerical residuals of computed variables. Residual monitor plots of conserved variables such as the mass, momentum and energy against the iteration number are very useful for judging the convergence (or divergence) of a solution, and they are created automatically within every simulation. It is worthy to note that initial conditions affects convergence path and a converged solution is one that is nearly independent of meshing errors.

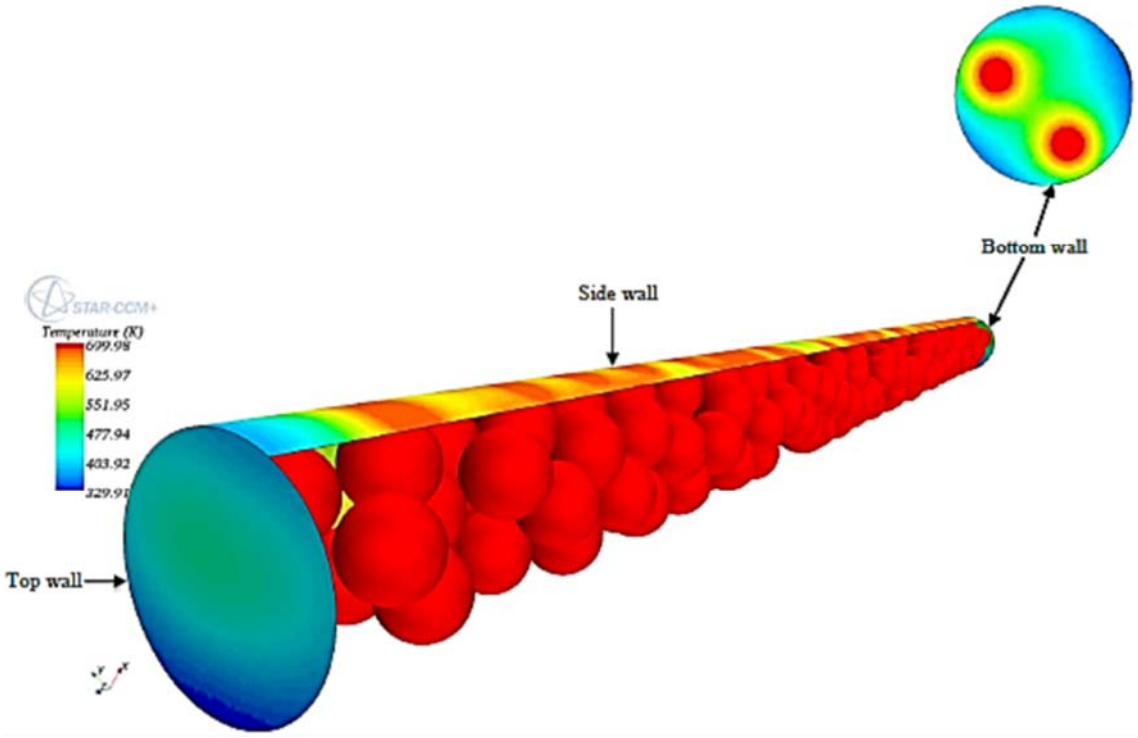

Fig. 5. Temperature contour plot for packed beds in helium environment contained in an enclosed slender cylindrical tube

4.4 Modeling Thermal Radiation.

Radiation model can be involved in fluid flow and thermal analysis. It is a heat transfer by electromagnetic waves; either wavelength-dependent (multiband radiation) or wavelength-independent (gray thermal radiation) that purely depends on surface temperatures, material properties, transmission media, and topology of the geometry. In modeling thermal radiation for this study, knowing that the solid is interfaced with the fluid domain hence surface-to-surface radiation is modeled on the fluid domain while the outside boundaries of the fluid are made transmissive so that they do radiatively interact. Only the fluid boundaries that are interfaced with the solid radiate to ambient. Under this circumstance, the amount of radiation received and emitted by each surface is uniquely defined by the surface's radiation properties and the thermal boundary conditions imposed on it. The surface properties are quantified in terms of emissivity, reflectivity, and transmissivity radiation temperature. These properties are not dependent on direction. Min/max temperatures for the fluid and solid continua are set to the same value as

appropriate for the run. When radiation properties are invariant with wavelength, the radiation is said to be gray. Gray radiation in this study is modeled using the gray thermal radiation model selection. The radiation properties are taken to be same over the entire thermal spectrum, and only a single radiative transfer solution is necessary for the full thermal spectrum.

4.5 Heat Transfer and Media Flow Model Analysis.

Simulations of HTR performance have been carried out by different authors using different simulation techniques and results analyzed. These techniques have been looked into before the commencement of this study and the most practicable simulation technique closer to the exact solution is adopted in this study. Results of the CFD simulations are presented first in the form of temperature contour plots and velocity vector plots to illustrate the qualitative features and insight that can be obtained. Following the qualitative discussion, CFD data are extracted to generate parameter plots that define the heat transfer performance in the medium. In this investigation, the heat transfer coefficient h_{pf}, Nusselt number Nu, and Rayleigh number Ra are the basic parameters used to evaluate and validate the convective heat transfer characteristics and transport in the packed bed considered.

Although Fig. 5 is modeled in a vertical direction but it is displayed in a horizontal direction for better description of its temperature contours. Figure 5 depicts temperature contours for the simulated packed beds. It can be seen that particles surface temperature in red contours are uniform but the side, top, and bottom outer walls temperatures are nonuniform. On the side walls, the reddish-brown contours show the influence of conduction at each particle-to-wall point contact and the heat spread out by the yellow contours on the side walls from these contacts is due to the influence of the hot helium gas neighboring the wall boundary along axial direction. The blue/green contours on the outer side wall close to the top and bottom of the tube are influenced by the gas temperature and heat transfer spread out along the tube wall at these two locations.

The tube top wall surface located on the extreme left of the modeled diagram has no particle point contact on its surface hence the greenish contours indicate the influence of less dense hot helium gas experiencing recirculation concentrated on

one part of the top wall boundary while areas with blue contours indicate the influence of hot gas not experiencing recirculation. This can be confirmed by the heat spread out on the top wall surface which is seen to be nonuniform as one side of the surface receives more heat than the other and this is proved to be true by the velocity vector plot. The two red contours on the bottom wall located at the extreme right of the modeled diagram indicate the influence of just two particle points contact on the bottom wall surface. The yellow/green/blue contour is an influence of heat spread out from the two heated point contacts being assisted by the hot gas neighboring the wall boundary. The hot helium gas helps to improve the conduction heat transfer from the coated particle fuel to the cladding tube walls thereby creating a heat spread out on the tube walls.

A velocity vector plot is created by defining a 2D plane. The resulting dataset consists of all the elements that intersect the defined plane so that the data to be shown are not obscured by elements in front of the plane of view. The velocity vectors are colored according to their magnitudes, and their lengths are projections of the 3D fluid flow vectors onto the defined plane. Figure 6(a) shows a vertical section over the whole bed height, through the bed center, and extending to two particle diameters in the radial direction. The section illustrates the bulk gas movement due to fluid temperature difference developed immediately after the simulation run, the initial heat supplied to the fluid created a sudden change in the medium gas density. A scenario shortly after the simulation run is depicted in Fig. 6(b) depicts. From the yellow/green contours, the area of highest flow is observed to be in the bed center while noticeable flow recirculation is gradually developing at the extreme corners of the top wall. As the gas temperature increases, flow recirculation at specific locations in the medium becomes fully developed as seen in Fig. 6(c). With flow recirculation now fully developed, bulk gas movement is seen to drop tremendously in the medium (see Fig. 6(c)) as bulk helium gas temperature approaches particle surface temperature while simulation progresses toward the end.

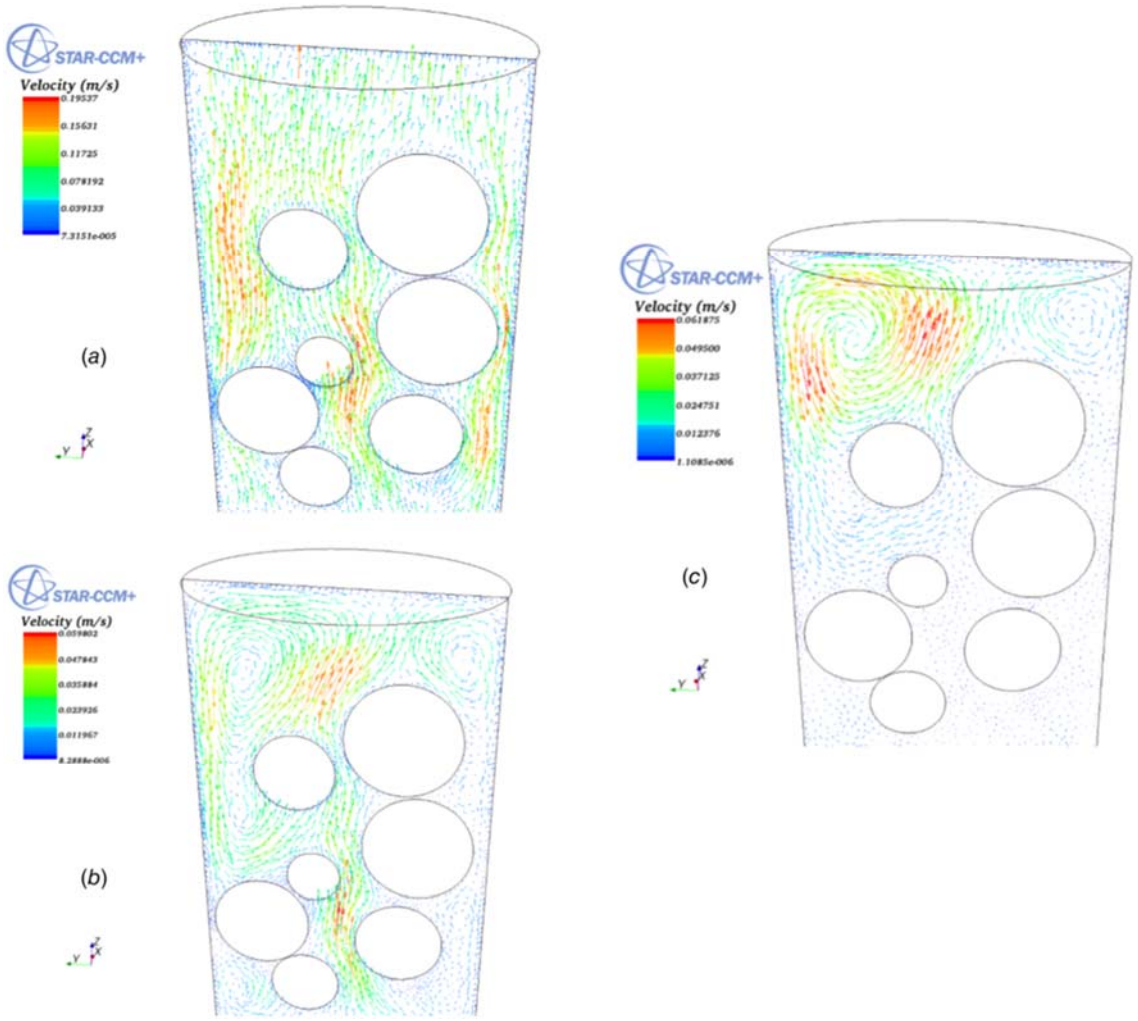

Fig. 6. (*a*) Sectional plane velocity vector plot immediately after the startup of the simulation run, (*b*) sectional plane velocity vector plot shortly after startup of the simulation run, and (*c*) sectional plane velocity vector plot before the end of the simulation process

A mesh sensitivity analysis performed and depicted graphically in Fig. 7 involves changing mesh density in the regions in order to properly capture the boundary layer-associated problems. Four sets of simulations were carried out within specified temperature range using varying mesh density and temperature profile results plotted. It is seen that as the temperature plot for the mesh density increases from 0.5 to 2.0, the lines move closer and closer indicating a transition from coarse to finer grid mesh refinement, the physical appearance of the mesh geometries also attest to this. As mesh density increases, fitting with theoretical solution improves; results obtained for the two finer meshes (1.5 and 2.0) are very close, so it can be established that simulations have reached an asymptotic solution. Optimum mesh density of 2.0 at the particle surface is used to build the mesh for the fixed bed

model. Packed particle temperature is measured along the axial and radial direction to determine temperature uniformity along the directions. Figure 8 illustrates particles temperature along the axial length to be uniform except for a slight drop for the first particle in contact with the bottom wall which may be due to heat loss to the contacting bottom wall through conduction. Likewise, particle temperature along the radial direction for the three locations examined is relatively uniform except for a slight drop for particles in contact with the side walls. This may also be attributed to heat loss to contacting walls on both sides through conduction.

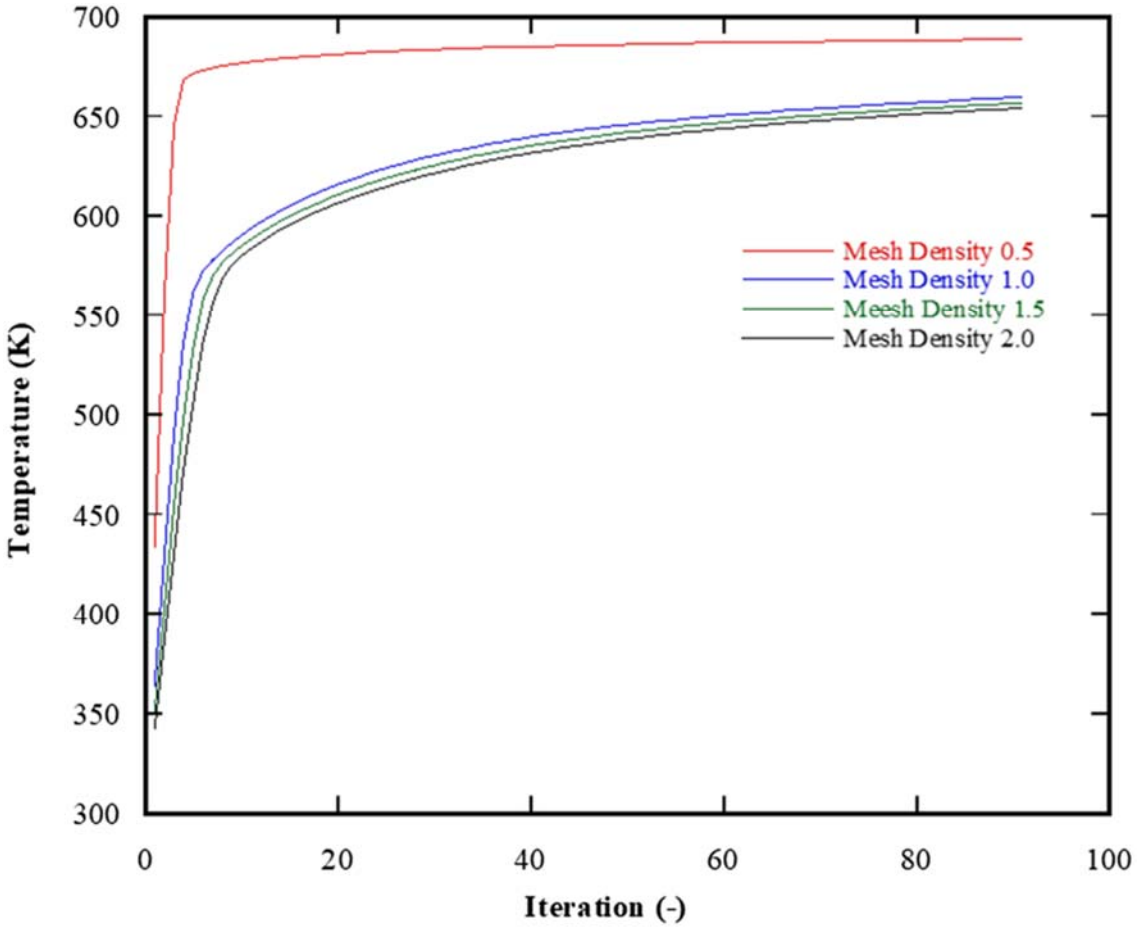

Fig. 7. Mesh sensitivity analysis

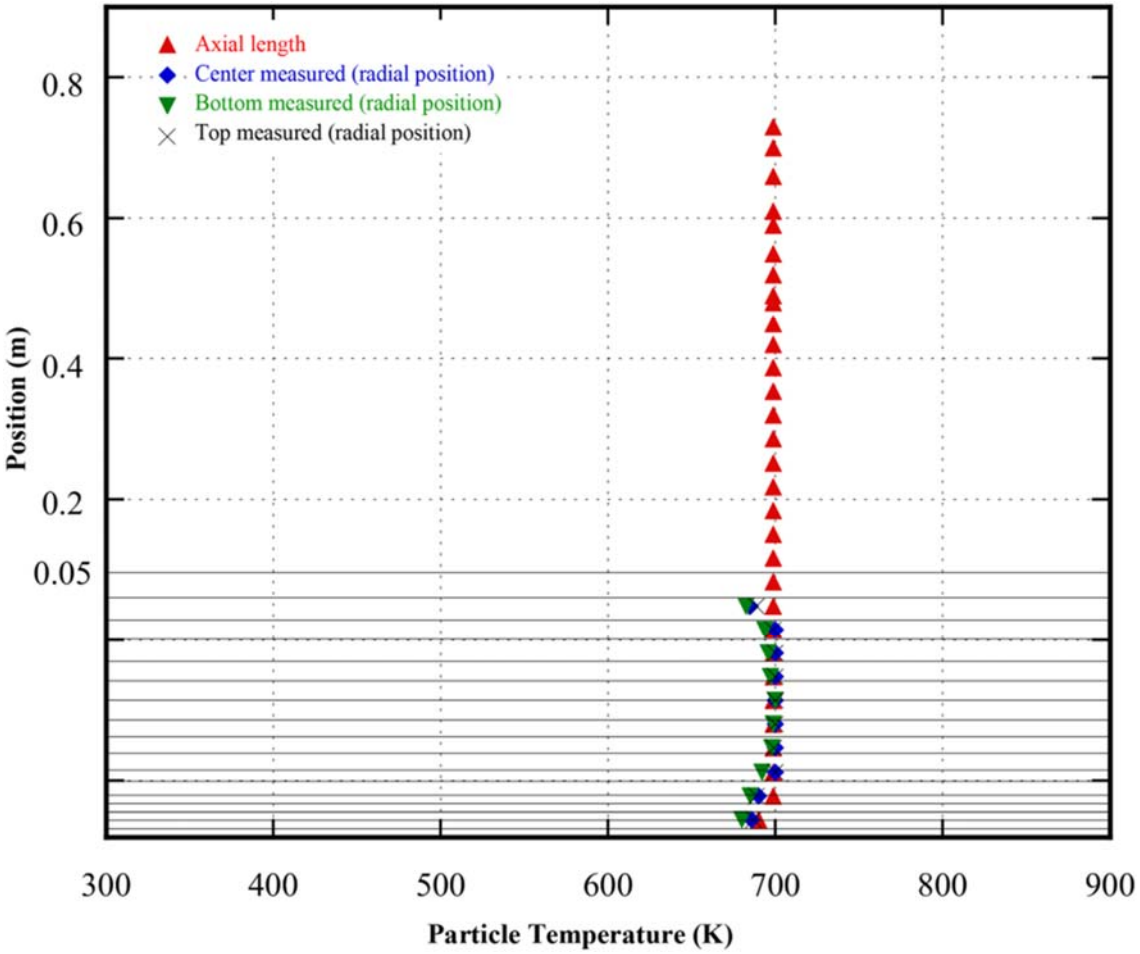

Fig. 8. Particle temperature profile along axial and radial positions

5 Results and Discussion

Unlike in HTR where continuous passage of cooling fluid (helium gas) is carried out in the reactor, the proposed design has both ends of the cladding tightly closed (see Fig. 1(c)) with the working fluid and packed coated particle fuel contained in it. It should be noted that the helium gas trapped in the cladding tube is basically to enhance heat transfer and not for cooling purpose as obtainable in HTR. Results of the heat transfer performance and medium fluid flow are displayed graphically for analysis. Validation of these results with other experimental and numerical results in literature is carried out to ascertain their level of agreement with existing works. Errors and uncertainty are unavoidable aspects of CFD modeling. Such errors and uncertainty could emanate from round-off error (error caused by computational representation of real numbers by means of a finite number of significant digits), iterative convergence error (numerical errors resulting from truncating the iteration of

discretized governing equations before final or exact solution is reached), discretization error (error from representing a function by its values at a discrete set of points), input uncertainty (inaccuracies due to limited information or approximate representation of geometry, boundary conditions, fluid/material properties), and physical model uncertainty (discrepancies between real flows and CFD due to inadequate representation of physical/chemical processes or due to simplifying assumptions in the modeling process). Some of these errors and uncertainties are quantified in the study and appropriate measures were taken to reduce them to the barest minimum during the simulation process.

5.1 Heat Transfer and Transport Validation.

The present work was validated with experimental and numerical results of a number of researchers involved in similar investigation of heat transfer and transport phenomena in packed beds. In the present work, a plot of increasing fluid temperature rise against particle-to-fluid heat transfer coefficient is depicted in Fig. 9. The graph shows a sudden initial rise in heat transfer coefficient followed by a plunge after the gas had gained some substantial heat and later a gradual drop until around 600 K when a rise in the heat transfer coefficient started developing again. The initial rise in heat transfer coefficient could be attributed to a sudden high heat input on particle surfaces due to nuclear fission reaction. The initial sudden high heat input created a sharp drop in fluid density resulting in an initial high convective fluid velocity (see Fig. 6(a)). As fluid temperature rose, flow recirculation began to develop at various locations while convective fluid velocity was on the decline (see Fig. 6(b)) due to reducing buoyancy force acting on the gas. This transformed into a decreasing heat transfer coefficient, as shown in Fig. 9. The surrounding water on the outside of the tube prevented a condition of local thermal equilibrium from being reached in the medium as heat transfer coefficient gradually rises to attain a steady value.

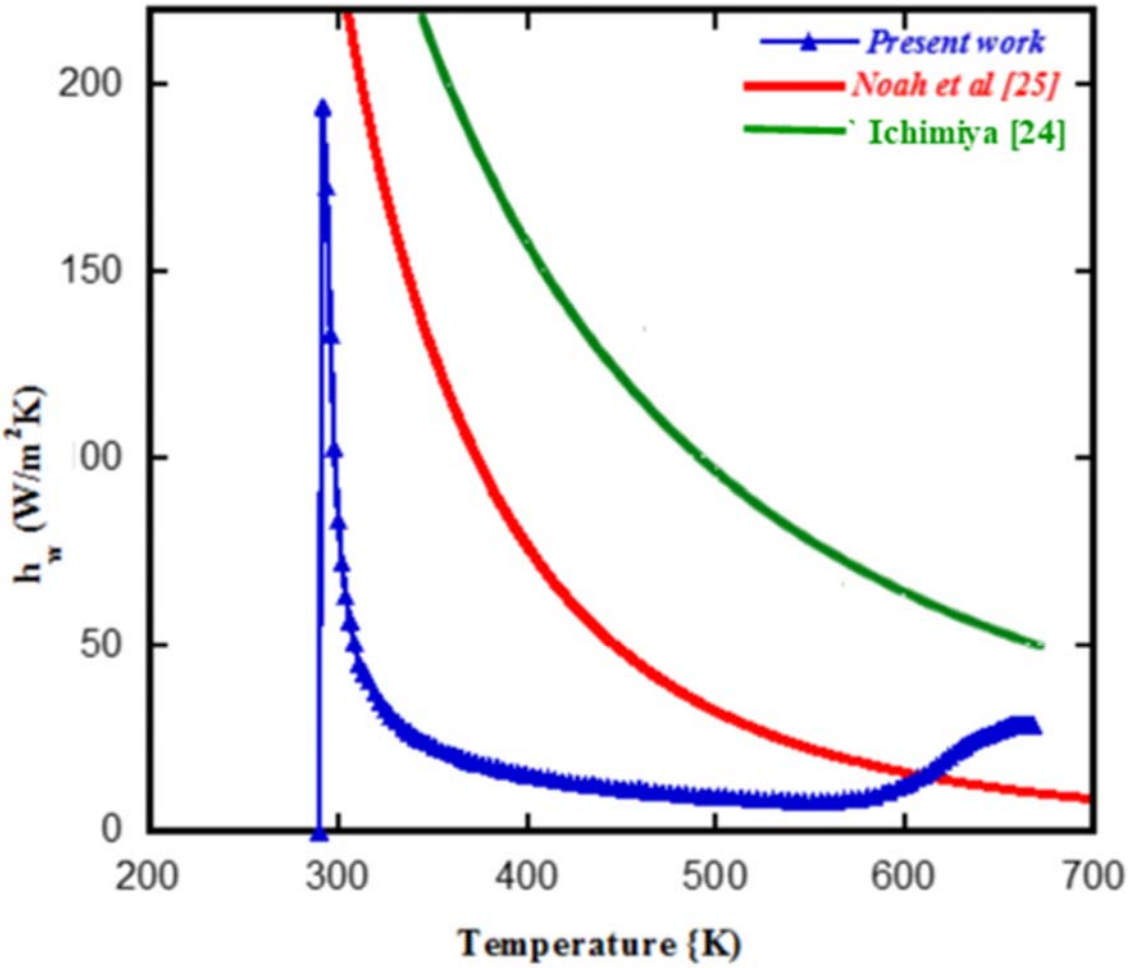

Fig. 9. Comparison of the effect of convective fluid velocity on particle-to-fluid heat transfer coefficient by direct simulation of spherical packings permeated by fine-scale voids and a porous region modelling

To validate the effect of convective fluid velocity on particle-to-fluid heat transfer coefficient the present work is compared with the work of Noah et al. [23] where the porous region modeling approach is applied. The latter work simulates an enclosed cavity fluid-saturated porous region where lumped parameter effect is involved and medium properties are defined. Although the present work could be said to be in fairly good agreement with the work of Noah et al. [23] but it is observed that gradual decline in heat transfer coefficient is not as steep as obtained in the present work. This could be due to the inability of the porous region modeling approach adopted by Noah et al. [23] to capture fine-scale voids that permit the passage of fluids in the enclosure and both cases the surrounding water on the outside of the tube prevents a condition of local thermal equilibrium from being reached in the

medium. The work of Ichimiya [24] which involves an application of a new method in estimating the heat transfer coefficient between fluid gas and solid materials in a porous medium is observed also to be in fairly close agreement with the present work. The high heat transfer coefficient obtained with this new method is likely due to indirect measurement of solid and fluid temperatures in the medium during the experiment.

The present work in Fig. 10 depicts a sharp rise in surface average gas velocity occurring due to a sharp fluid temperature rise caused by a sudden high heat input on particle surfaces immediately after the fission reaction began. The initial sharp rise in the convective surface average gas velocity was responsible for the initial sharp rise in the particle-to-fluid heat transfer coefficient observed in Fig. 9. The graph in Fig. 10 is related to that in Fig. 9 because h_{pf} is a function of the flow around the particle surfaces. The rise was short-lived as the gas velocity was seen to drop abruptly before rising again to a fair stable value as the simulation progressed. The accuracy and stability achieved in the work of du Toit et al. [25] in comparing predicted experimental results of SANA test cases with numerical result using systems CFD code made it suitable for validation of the present work. Although the present work is observed to be in agreement with the work of du Toit et al. [25] but it should be noted that the present work has its helium gas trapped in the cladding tube while that used by du Toit et al. [25] flows from the point of entry out and is discharged out at the point of exit. This necessitated the low fluid velocity in the present work coupled with the large particle diameter considered by du Toit et al. [25] comparable to the small particle size used in the present work. The work of Logtenberg and Dixon [11] also observed in Fig. 10 is in fair agreement with this work through it exhibits slight increase in fluid velocity as temperature in the medium increases.

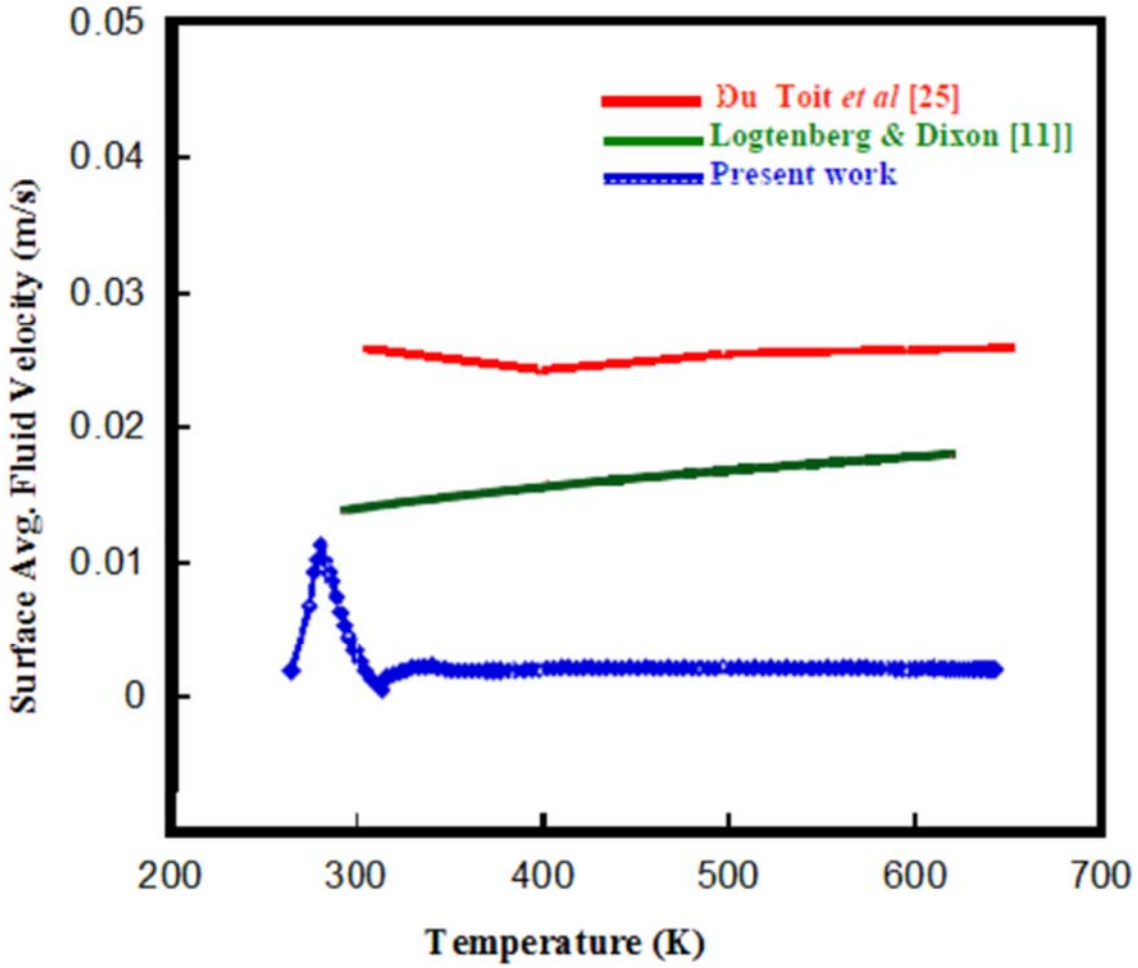

Fig. 10. Comparison of the effect of natural convective flow in fixed beds

Figure 11 depicts the changes in the Nusselt number with respect to the heat transfer between heat-generating particles and hot helium gas. The rise in Nusselt number in the present work is ascribed to initial high heat input on particle surfaces resulting from nuclear fission reaction. At the initial heating stage of the gas by the particles, convective fluid velocity was on the rise due to reducing gas density at an increasing gas temperature. As gas temperature increased, convective fluid velocity started dropping due to reducing buoyancy force acting on the gas. The surrounding water on the outside of the tube prevented a condition of local thermal equilibrium from being reached in the medium. While the dimensionless Reynolds number (Re) governs the flow regime in forced convection, the flow regime in natural convection is governed by the dimensionless Grashof number (Gr), which represents the ratio of the buoyancy force to the viscous force acting on the fluid. The Rayleigh number

which is associated with buoyancy-driven flow increases along with the Nusselt number as seen in Fig. 11. As fluid temperature increases further, flow recirculation began to develop at various locations while convective fluid velocity declines. It is observed at this point that Nusselt number begins to drop with decreasing Rayleigh number.

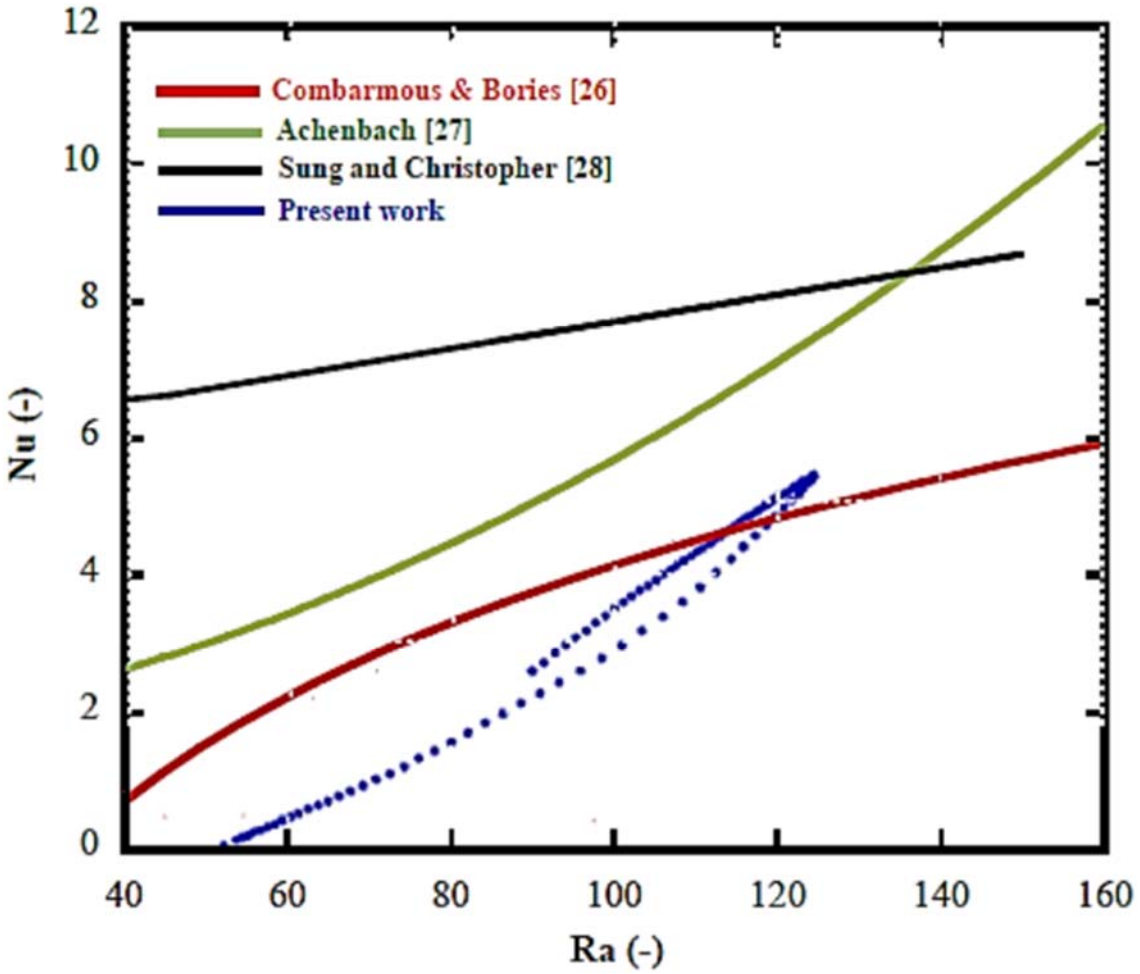

Fig. 11. Comparison of the effect of Nusselt number against Rayleigh number for particle-to-fluid heat transfer

The work of Combarmous and Bories [26] was used in validating this work. A gradual increase in Nusselt number with increasing temperature observed in the later work could be attributed to the medium being a horizontal layer and channel being open at both ends. Considered also are the work of Achenbach [27], Sung and Christopher [28]. The result of experimental work of Achenbach on particle-to-fluid heat transfer and flow in beds of nonuniform porosity shows that, with an increasing temperature and fluid flow, the Nusselt number increases with an increasing Rayleigh number for

an unenclosed cavity. The numerical investigation by Sung and Christopher [28] of the effect of Raleigh number and aspect ratio on the buoyancy-induced convection when a porous layer underlying a fluid layer is heated from below reveals a steady rise in Nusselt number with an increasing Raleigh number. The case of the present study is unique due to enclosure of the medium at both ends given rise to flow recirculation.

6 Conclusion and Recommendations

This work is a contribution to global research to make water-cooled reactors safer. An innovative nuclear fuel design was proposed and investigated. The introduction of coated fuel particles as an accident tolerant fuel for water-cooled reactors could promote water-cooled reactors as a candidate for generation IV reactor systems [29]. CFD has proven to be a reliable tool for modeling fixed bed reactors [2] through the resolution of 3D transport equations for mass, momentum, and energy balances. Solution of these equations has enabled the velocity and temperature profiles within the mimicked cladding attainable. The comparison between established numerical data and the present simulations reported here provides validation for the use of CFD to compute heat transfer and transport phenomena over wide temperature range. The new concept of direct particle-to-particle and particle-to-wall contact model developed in this work by the combined use of CAD and commercial code helps resolved the convergence problem and thereby generate a better numerical solution. This new concept is an improvement over the existing bridge and caps methods as point contact is achieved similar to real-life application in the new adopted approach. From the comparison, it can be concluded that simulated results in this work are in close agreement with established numerical and experimental results.

Further work is recommended on the investigation of heat transfer performance from outer walls of the cladding tube to the surrounding cooling water. This will encompass complete analysis considering the heat transfer to the cladding and the flowing coolant outside of the fuel rod and then compare the result to the traditional fuel design.

Funding Data

Department of Mechanical and Aeronautical Engineering, University of Pretoria, Pretoria, South Africa, National Research Foundation.

Nomenclature

a =	specific surface area, m^{-1}
$\mathbf{a}$ =	face area vector, m^2
A =	area, m^2
$\mathbf{B}_f$ =	body force, N
C =	concentration, (kg/kg)
c_p =	specific heat at constant pressure, J/kg K
d =	diameter, m
F =	contact force between two particles, N
g =	gravity, m/s^2
h =	heat transfer coefficient, W/m^2 K
k =	thermal conductivity, W/m K
k_n =	normal stiffness
L =	bed height, m
m =	reduced mass of particle
N =	normal part of the force, F (N)
N =	diameter ratio, (d_b/d_p)
$\overline{N}_c$ =	average coordination number

P = pressure, Pa

P_i = inertial resistance coefficient

P_v = viscous resistance coefficient

q = heat transfer, J

Q = rate of heat transfer, W

q'' = heat flux, W/m^2

r = radius, m

r = radial coordinate, m

R = thermal resistance, K/W

$S_\emptyset$ = scalar source term

T = temperature, K

u = velocity, m/s

$\mathbf{v}$ = velocity vector, m/s

V = volume, m^3

z = axial coordinate, m

Greek Symbols

α = damping parameter (dimensionless)

β = thermal expansion coefficient, $1/\mathrm{K}$

β_t = tangential viscosity parameter (Ns/m)

Γ = diffusion coefficient

δ = distance between two particles, m

$\dot{\delta}$ = sliding velocity (m/s)

ε = porosity

μ = dynamic viscosity, $Ns^{-1}m^{-2}$

μ_c = friction coefficient

v = kinematic viscosity, m^2/s

ρ = density, kg/m^3

$\overrightarrow{\overline{\tau}}$ = stress tensor, Pa

∞ = lower bulk

Subscripts

c = contact point

eff = effective

f = fluid

G = macrogap

n = normal

p = particle

p = pressure

R = radiated

t = tangential

Superscript

c = contact interface between particles

Nondimensional Numbers

Gr =	Grashof number, $\frac{g\beta\lvert T_s - T_f\rvert d_p^3}{\nu^2}$
Nu =	Nusselt number, $\frac{h d_p}{k_f}$
Ra =	Rayleigh number, $\frac{g\beta\lvert T_s - T_f\rvert d_p^3}{\nu^2} \frac{\mu c_p}{k_f}$
Re =	Reynolds number, $\frac{\rho u d_p}{\mu}$

Acronyms

CAD =	computer aided design
CFD =	computational fluid dynamics
DEM =	discrete element method
HTR =	high temperature reactor
LWRs =	light-water reactors
SiC =	silicon carbide

References

1. Janse van Rensburg, J. J. , and Hoffmann, J. E. , 2006, " CFD Modeling of the PBMR Reactor Unit," *Proceedings of the Third International Topical Meeting on High Temperature Reactor Technology (HTR2006)*, Johannesburg, South Africa, Oct. 1–4, p. 238.

2. Guardo, A. , Coussirat, M. , Recasens, F. , Larrayoz, M. A. , and Escaler, X. , 2006, " CFD Study on Particle- to-Fluid Heat Transfer in Fixed Bed Reactors: Convective Heat Transfer at Low and High Pressure," *Chem. Eng. Sci.*, 61(13), pp. 4341–4353.10.1016/j.ces.2006.02.011

3. Kta, S. , 1978, " Reactor Core Design of High Temperature Gas-Cooled Reactors," Nuclear Safety Standards Commission, Germany, KTA Standard Nos. 3102.1, 3102.2, 3102.3 (1983, 1981).

4. Noah, O. O. , Slabber, J. F. , and Meyer, J. P. , 2015, " Investigation of Natural Convection Heat Transfer Phenomena in Packed Beds: Lead-Way Towards New Nuclear Fuel Design," *ASME J. Nucl. Eng. Rad. Sci.*, 1(4), p. 041014.10.1115/1.4030983

5. Shams, A. , Roelofs, F. , Komen, E. M. J. , and Baglietto, E. , 2013, " Quasi-Direct Numerical Simulation of a Pebble Bed Configuration: Part 1: Flow (Velocity) Field Analysis," *Nucl. Eng. Des.*, 263, pp. 473–489.10.1016/j.nucengdes.2012.06.016

6. Zeiser, T. , Lammers, P. , Klemm, E. , Li, Y. W. , Bernsdorf, J. , and Brenner, G. , 2001, " CFD Calculation of Flow, Dispersion and Reaction in a Catalyst Filled Tube by the Lattice Boltzmann Method," *Chem. Eng. Sci.*, 56(4), pp. 1697–1704.10.1016/S0009-2509(00)00398-5

7. Augier, F. , Idoux, F. , and Delenne, J. Y. , 2010, " Numerical Simulation of Transfer and Transport Properties Inside Packed Beds of Spherical Particles," *Chem. Eng. Sci.*, 65(3), pp. 1055–1064.10.1016/j.ces.2009.09.059

8. Calis, H. P. A. , Nijenhuis, J. , Paikert, B. C. , Dautzenberg, F. M. , and van den Bleek, C. M. , 2001, " CFD Modeling and Experimental Validation of Pressure Drop and Flow Profile in a Novel Structured Catalytic Reactor Packing," *Chem. Eng. Sci.*, 56(4), pp. 1713–1720.10.1016/S0009-2509(00)00400-0

9. Romkes, S. J. P. , Dautzenberg, F. M. , van den Bleek, C. M. , and Calis, H. P. A. , 2003, " CFD Modeling and Experimental Validation of Particle-to-Fluid Mass and Heat Transfer in a Packed Bed at Very Low Channel to Particle Diameter Ratio," *Chem. Eng. J.*, 96(1–3), pp. 3–13.10.1016/j.cej.2003.08.026

10. Derkx, O. R. , and Dixon, A. G. , 1996, " Determination of the Fixed Bed Wall Heat Transfer Coefficient Using Computational Fluid Dynamics," *Numer. Heat Transfer Part A*, 29(8), pp. 777–794.10.1080/10407789608913819

11. Logtenberg, S. A. , and Dixon, A. G. , 1998, " Computational Fluid Dynamics Studies of Fixed Bed Heat Transfer," *Chem. Eng. Process*, 37(1), pp. 7–21.10.1016/S0255-2701(97)00032-9

12. Logtenberg, S. A. , Nijemeisland, M. , and Dixon, A. G. , 1999, " Computational Fluid Dynamics Simulations of Fluid Flow and Heat Transfer at the Wall-Particle Contact Points in a Fixed-Bed Reactor," *Chem. Eng. Sci.*, 54(13–14), pp. 2433–2439. 10.1016/S0009-2509(98)00445-X

13. Nijemeisland, M. , and Dixon, A. G. , 2001, " Comparison of CFD Simulations to Experiment for Convective Heat Transfer in a Gas–Solid Fixed Bed," *Chem. Eng. J.*, 82(1–3), pp. 231–246.10.1016/S1385-8947(00)00360-0

14. Suzuki, M. , Makino, K. , Yamada, M. , and Iinoya, K. , 1981, " A Study on the Coordination Number in a System of Randomly Packed, Uniform-Sized Spherical Particles," *Int. Chem. Eng.*, 21, pp. 482–488.

15. Cundall, P. A. , and Strack, OD. I. , 1979, " A Discrete Numerical Model for Granular Assemblies," *Geo Tech.*, 29(1), pp. 47–65.10.1680/geot.1979.29.1.47

16. Delenne, J.-Y. , El Youssoufi, M. S. , Cherblanc, F. , and Bénet, J.-C. , 2004, " Mechanical Behavior and Failure of Cohesive Granular Materials," *Int. J. Numer. Anal. Methods Geomech.*, 28(15), pp. 1577–1594.10.1002/nag.401

17. CD-Adapco, 2012, "*CCM+ User Guide 7.02, Setting Material Properties Methods*," Melville, NY, p. 2463.

18. Soulie, F. , Cherblanc, F. , El Youssoufi, M. S. , and Saix, C. , 2006, " Influence of Liquid Bridges on the Mechanical Behaviour of Polydisperse Granular Materials," *Int. J. Numer. Anal. Methods Geomech.*, 30(3), pp. 213–228.10.1002/nag.476

19. Richefeu, V. , El Youssoufi, M. S. , and Radjai, F. , 2006, " Shear Strength Properties of Wet Granular Materials," *Phys. Rev. E*, 73(5), p. 051304.10.1103/PhysRevE.73.051304

20. Allen, M. P. , and Tildesley, D. J. , 1986, *Computer Simulation of Liquids*, Oxford University Press, Oxford, UK.

21. Spalart, P. R. , 2000, " Strategies for Turbulence Modeling and Simulations," *Int. J. Heat Fluid Flow*, 21(3), pp. 252–263.10.1016/S0142-727X(00)00007-2

22. Shur, M. , Spalart, P. , Squires, K. , Strelets, M. , and Travin, A. , 2005, " Three Dimensionality in Reynolds-Averaged Navier–Stokes Solutions Around Two Dimensional Geometries," *AIAA J.*, 43(6), pp. 1230–1242.10.2514/1.9694

23. Noah, O. O. , Slabber, J. F. , and Meyer, J. P. , 2016, " Modeling a Porous Region for Natural Convection Heat Transfer and Experimental Validation in Slender Cylindrical Geometries," *Nucl. Technol.*, 193(3), pp. 375–390.10.13182/NT15-56

24. Ichimiya, K. , 1999, " A New Method for Evaluation of Heat Transfer Between Solid Material and Fluid in a Porous Medium," *ASME J. Heat Transfer-Trans. ASME*, 121(4), pp. 978–983.10.1115/1.2826089

25. Du Toit, C. G. , Rousseau, P. G. , Greyvenstein, G. P. , and Landman, W. A. , 2006, " A System CFD Model of a Packed Bed High Temperature Gas-Cooled Nuclear Reactor," *J. Therm. Sci.*, 45(1), pp. 70–85.10.1016/j.ijthermalsci.2005.04.010

26. Combarnous, M. , and Bories, S. , 1974, " M'odelization de la Convection Naturelle au Sein D'unecouche Poreuse Horizontale ′a L'aide D'un Coefficient de Transfert Solide-Fluide," *Int. J. Heat Mass Transfer*, 17(4), pp. 505–515.10.1016/0017-9310(74)90027-1

27. Achenbach, E. , 1995, " Heat and Flow Characteristics of Packed Beds," *Exp. Therm. Fluid Sci.*, 10(1), pp. 17–27.10.1016/0894-1777(94)00077-L

28. Sung, J. K. , and Christopher, Y. C. , 1995, " Convective Heat Transfer in Porous and Overlying Fluid Layers Heated From Below," *Int. J. Heat Mass Transfer*, 39(2), pp. 319–329.10.101/0017-9310(95)00118-S

29. Noah, O. O. , Slabber, J. F. , and Meyer, J. P. , 2019, " Introducing Passive Nuclear Safety in Water-Cooled Reactors - Numerical Simulation and Validation of Natural Convection Heat Transfer and Transport in Packed Beds of Heated Microspheres," ASME Paper No. ICONE27-1383.